IEEE Access
Multidisciplinary | Rapid Review | Open Access Journal

Received October 6, 2019, accepted October 30, 2019, date of publication November 6, 2019, date of current version November 15, 2019.

Digital Object Identifier 10.1109/ACCESS.2019.2951763

Automatic Vehicle-Pedestrian Conflict Identification With Trajectories of Road Users Extracted From Roadside LiDAR Sensors Using a Rule-Based Method

BIN LV[1], RENJUAN SUN[2], HONGBO ZHANG[2], HAO XU[3], AND RUI YUE[3]

[1]School of Traffic and Transportation, Lanzhou Jiaotong University, Lanzhou 730070, China
[2]School of Qilu Transportation, Shandong University, Jinan 250061, China
[3]Department of Civil and Environmental Engineering, University of Nevada, Reno, NV 89557, USA

Corresponding authors: Bin Lv (jdlbxx@mail.lzjtu.cn) and Rui Yue (ruiyueunr@gmail.com)

This work was supported in part by the Natural Science Foundation of China under Grant 61463026 and Grant 61463027, and in part by the Foundation of A Hundred Youth Talents Training Program of Lanzhou Jiaotong University.

ABSTRACT Vehicle-pedestrian conflicts have been the major concern for traffic safety. Surrogate safety measures are widely applied for pedestrian safety evaluation. However, how to quickly identify the vehicle-pedestrian surrogate safety measures at the individual site is challenging due to the difficulty of obtaining the high-resolution trajectories of road users. This paper presented an effective method to generate the high-resolution traffic trajectories from the roadside deployed Light Detection and Ranging (LiDAR) sensor. The vehicle-pedestrian conflicts can then be identified from the trajectories simply using the speed-distance profile (SDP) of the vehicles. The SDP can be used to develop a rule-based method for vehicle-pedestrian identification. The events can be divided into different risk levels based on the spatial distribution of the SDP. The case study shows that the rule-based method can detect vehicle-pedestrian near-crash events effectively. The other indicators, such as widely used time-to-collision (TTC) or deceleration rate to avoid a crash (DRAC), can be also obtained from the SDP. The engineers can also adjust the thresholds in the rule-based method to meet the specific requirements at different sites. The proposed method can be extended to identify vehicle-vehicle conflicts or vehicle-bicycle conflicts in future studies.

INDEX TERMS Roadside LiDAR, vehicle-pedestrian conflicts, surrogate safety measures, high-resolution trajectories, pedestrian safety.

I. INTRODUCTION

Pedestrians are vulnerable groups on the roads compared to motor vehicles. The vehicle-pedestrian conflict has been a major concern of public health worldwide [1]. According to the traffic safety facts released by National Highway Traffic Safety Administration (NHTSA), a total of 79,000 pedestrians were involved in vehicle-pedestrian crashes, including 5,977 fatalities in the United States in 2017 [2]. Intersections have been the most dangerous traffic element for pedestrians due to the complex traffic conflicting movements [3]. For unsignalized intersections, pedestrians need to make a go/waiting decision when they reached or are close to the crossing line [4]. Due to aggressive driving behavior or driving distraction, drivers may fail to yield to pedestrians at unsignalized intersections, which can result in severe crashes [5]. For signalized intersections, pedestrians crossing the road may have conflicts with right-turn-on-red vehicles or left-turn-on-green vehicles [6]. How to assess the status of pedestrian safety and to provide the corresponding countermeasures for pedestrian safety improvements are important tasks for traffic engineers. The most common approach for vehicle-pedestrian conflicts analysis is the crash-based method; however, the frequency of vehicle-pedestrian crashes

The associate editor coordinating the review of this manuscript and approving it for publication was Yongquan Sun.

This work is licensed under a Creative Commons Attribution 4.0 License. For more information, see http://creativecommons.org/licenses/by/4.0/

is lower than other crash types [7]. Therefore, it is usually difficult to obtain adequate crashes to perform the crash-based evaluation at a specific site. Furthermore, the detailed descriptions of the crash (e.g., crash time, driver behavior, and pedestrian movements) usually rely on the investigating officers' judgment and the involved road users' self-reports. It could not be guaranteed that the actual situation of the crash is recorded and human errors are inevitably included in the crash statistics. Surrogate safety measures are widely applied in traffic safety analysis [8]. In general, a surrogate safety measure refers to the situation that two or more road users would collide or be near-collision if they remain on their paths or speeds on the roads [9]. Though crashes and surrogate safety measures are two different types of events, the previous study [3] already showed that using surrogate safety measures can be used for conflict analysis when the historical crash data were not available.

Different types of data collection methods for surrogate safety measures have been developed by previous researchers, including site-based methods [10], simulation-based methods [11], and naturalistic driving studies (NDS) [12]. Manual observation might be the first site-based method. For manual observation, the vehicle-pedestrian conflicts were observed in the field and the details of the conflicts were recorded and post-processed [13]. Since manual observation in the field was time-consuming and labor-intensive, other types of site-based methods were then developed. The most widely used site-based method is video detection technology [14]. Sayed *et al.* developed a computer-based method for vehicle-bicycle conflict identification from video detectors [15]. The computer vision module mainly includes feature detection, tracking, grouping, and classification. The safety analysis module includes trajectory generation, patterns analysis, and conflicts identification. The case study shows that indicators, such as time-to-collision (TTC) can be successfully gained from the computer-based method. Ismail *et al.* [16] developed an automatic procedure that can extract the vehicle-pedestrian conflicts using video data. The indicators such as TTC, deceleration-to-safety time (DST), and post-encroachment-time (PET) can be calculated using the proposed method. Jiang *et al.* [17] analyzed the relationship between TTC and vehicle speed profile using the video data. It was found that the smaller TTC occurs when the driver chooses harder braking, whereas a larger TTC corresponds to a lower deceleration rate. Tageldin and Sayed developed evasive action-based indicators using video detectors [18]. Pedestrian evasive actions usually involve a sudden change in their walking mechanism. This reaction is reflected in the pedestrian gait parameters (step frequency and/or step length). Threshold: max absolute rate of change in step frequency > 0.7 steps/s2 and Jerk < -8 m/s3. The threshold was developed for a congested intersection. The transferability of the thresholds needs to be further investigated. Though the above-mentioned video-based studies indicated that video detection was a good method for vehicle-pedestrian conflicts data collection, the video-based method suffered a major limitation that the performance of video sensors can be greatly influenced by light conditions, especially during sunrise and sunset time.

Researchers have made efforts to analyze vehicle-pedestrian conflicts by investing the existing indicators or developing their indicators using the simulation-based method [19]. Gettman and Head [20] investigated the performance of different indicators from traffic simulation models. It was found that maximum speed and the speed differential are two indicators that can measure the risk level effectively. Ozbay et al. [21] developed and validated two new safety indicators: derived crash index (CI) and modified (TTC) using a calibrated simulation model. Wang and Stamatiadis [22] compared the performance of a simulation-based surrogate safety metric-aggregate conflict propensity metric (ACPM) with TTC and found ACPM can provide the results highly consistent with the Highway Safety Manual (HSM). The high correlation between simulated and field-measured conflicts was found after calibration [23]; however, the calibration parameters varied considerably among different traffic environments, meaning extract efforts were required to calibrate the models in different situations. Therefore, simulation-based methods can be a good approach to analyze vehicle-pedestrian conflicts under a specific environment, and to validate the performance of different indicators, but may not be effective to assess pedestrian safety for massive real sites.

Surrogate safety measures extracted from NDS can provide drivers' and pedestrians' real behaviors at the occurrence of the conflicts [24]. The emerging use of naturalistic driving studies (such as the use of the Strategic Highway Research Program 2 database-SHRP 2) provides a good approach to capture the detailed and real surrogate safety measures. The NDS data can be extracted through a series of sensors installed on the vehicles, including but not limited to on-board cameras, radars, GPS, and accelerometers. Wu and Jovanis [25] used receiver operating characteristic (ROC) methods to extract the near-crash events from the Virginia Tech Transportation Institute (VTTI) 100-car study. Wang *et al.* [8] used a tree-based model to assess the driving risks using the near-crash database. Though the NDS data has a bunch of benefits, their application for site-based safety evaluation is still limited since the number of captured trips at the individual site is uncontrolled.

Other researchers using light detection and ranging (LiDAR) to generate the trajectories of road users for vehicle-pedestrian conflicts analysis [26]. Compared to the video sensor, the LiDAR can work day and night with the influence of different light conditions [27]. And the LiDAR doesn't have the problem of shade. The performance of the LiDAR can be reduced under rainy or snowy weather. But the researchers have improved the algorithms of detecting the objects under severe weather conditions using the LiDAR sensors [28]. Tarko *et al.* [29] investigated the feasibility of using LiDAR for safety analysis at intersections and concluded that the LiDAR sensor can provide high-resolution micro traffic data

(trajectories of all road users with second-by-second or even higher frequency) and can be a good option for vehicle-pedestrian conflicts collection. Zhao et al. [30] predicted the pedestrians' decision-crossing/not crossing the intersection using the trajectories extracted from the 360-degree LiDAR sensor deployed in a static location. A deep autoencoder-artificial neural network (DA-ANN) was applied to process the data and predict pedestrians' behaviors. About 95% prediction accuracy was achieved in the case study. However, that paper did not provide an effective method to identify the vehicle-pedestrian conflicts from the LiDAR data. Wu et al. [13] developed three indicators for vehicle-pedestrian near-crash identification using the roadside deployed LiDAR. The three indicators include time difference to the point of intersection (TDPI), distance between stop position and pedestrian (DSPP), and speed-distance profile. The field evaluation showed that a lot of ''false'' events (not near-crash events) were reported due to the undefined region of interest (ROI) and the occlusion issues in the LiDAR data. Therefore, the accuracy of vehicle-pedestrian conflicts identification algorithms or indicators in those LiDAR-related pioneer studies still needs to be further improved.

The limitations of previous studies related to vehicle-pedestrian conflicts are summarized as follows: 1. The resolution of the extracted trajectories used for surrogate safety measures analysis needs to be further improved. 2. The studies related to the site-based pedestrian safety assessment were limited. 3. The feasibility of the indicators (most of them were developed for vehicle-vehicle conflicts) on the vehicle-pedestrian conflicts analysis needs to be investigated systematically. This paper developed a systematical procedure to extract the high-resolution traffic data from the roadside LiDAR sensors. Those trajectories were then used as the input to evaluate the feasibility of different indicators. A new indicator, which was designed for vehicle-pedestrian conflicts especially, was also introduced and validated through case studies. The major contribution of this paper is that an automatic procedure for the vehicle-pedestrian conflicts is developed with its performance evaluated. The proposed method can be used at any site as long as the trajectories of vehicles and pedestrians are available. The extracted surrogate safety measures can be either used for pedestrian safety evaluation or be possibly used to develop the near-crash warning system for connected-vehicles since the real-time identification can be achieved in the future. The following parts of the paper are structured as follows. Section 2 documents the procedure of extracting high-resolution trajectories of road users from the roadside LiDAR. Section 3 introduces the speed-distance profile (SDP) designed for vehicle-pedestrian conflicts identification. Section 4 evaluates the performance of different indicators for vehicle-pedestrians conflict identification using real-world data. Section 5 discusses the major limitations of this research. The last section summarizes the findings and provides the research directions for future studies.

II. TRAJECTORIES EXTRACTION FROM ROADSIDE LIDAR

The high-resolution traffic data can benefit traffic safety, traffic operation, and a lot of other traffic aspects [49]. Unlike vehicle-vehicle conflicts which can last in a relatively long distance (such as rear-end near-crashes), the vehicle-pedestrian conflicts normally occurred at a limited area-crosswalk at the intersection. Therefore, the resolution of the trajectories can directly influence the identification of vehicle-pedestrian conflicts due to the short conflict time between the vehicles and pedestrians. The roadside LiDAR, also known as side-fire LiDAR or stationary LiDAR, has been an emerging application to providing the high-resolution traffic data for connected vehicles. The 360-degree LiDAR can create point clouds for its scanned objects with a high frequency (usually 5-20 Hz) in a wider range compared to radars or cameras [31]. Another reason why this research selected the roadside LiDAR was that the LiDAR can be easily installed on a tripod for temporarily data collection without many calibrations. This means pedestrian safety at the individual site can be assessed with the high-resolution trajectories extracted from 360-degree LiDAR.

A. TRAJECTORY EXTRACTION PROCEDURE

The whole data processing of the trajectory extraction contains parts: point registration, background filtering, point clustering, object classification, lane identification, and data association. Figure 1 shows the flow-chart of the data processing procedure.

The occlusion issue is the object blocking by another one can cause point loss in the roadside LiDAR. As a result, the shape of the object may be only partially visible or totally invisible. This issue has been reported by a bunch of studies [32]. One effective and simple solution to fixing the occlusion is installing another LiDAR at a different nearby location [33]. The LiDARs can have some overlapping areas, which can reduce the probability of full occlusion. Since each LiDAR reports the point cloud in a local system, it is necessary to integrate the point clouds into one unit coordinating system. This paper applied a revised iterative closest point (ICP) developed by the author in a previous study [34] for point registration among different LiDARs. Firstly, the algorithm synchronized the timestamp of different LiDARs using GPS time. Then at least three controlling points in the point cloud of each LiDAR were selected as the input of the ICP. The point pairs were integrated into a 2D space (XY coordinates) using the ICP. To find the best match in Z-axis, the ground surface was selected to adjust the offset in the height using the ICP. The two-point clouds from different LiDARs can be then integrated. The data integration step is optional since in real-world applications, not all LiDARs are linked with GPS and the occlusion issue may be weakened by selecting an appropriate height for the LiDAR installation.

The definition of ''background'' here is the object unrelated to road users in the space. More specifically speaking, the background includes buildings, trees, as well as ground points. Background filtering is to identify and exclude

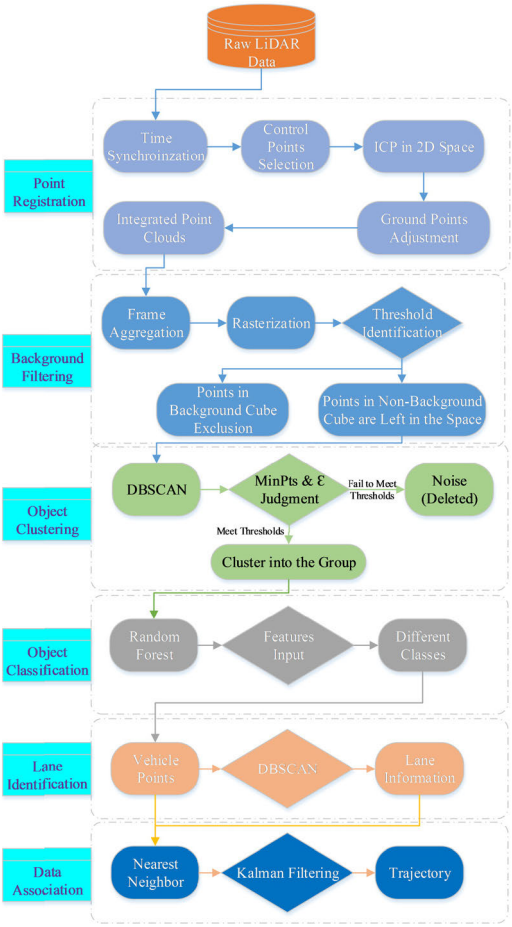

FIGURE 1. Flow chart of data processing algorithm.

backgrounds, which is an important step for LiDAR point reduction [35]. The background filtering can accelerate the following data processing steps by removing the irrelevant points from the space. The proposed background filtering algorithm includes three major parts: frame aggregation, rasterization, and threshold identification. For one frame, without comparing to other frames, it is difficult to know which cube represents background when there are moving objects in the space. By aggregating multiple frames (1500∼3500 frames) into one coordinate based on the XYZ location, the density of background points should be higher than that of non-background points. The whole space can be then rasterized into small cubes with the same side length. By giving a pre-defined threshold of point density for each cube, the cube can be identified as background cube or non-background cube. The location of the background points can be then stored in a 3D array (containing the spatial location with XYZ). Any points detected in the 3D array are identified as background points and are excluded from the space. The detailed background algorithm can be found from an earlier version [35] and a later improved version [36].

The purpose of object clustering is to group the points belonging to one object into one cluster. The density-based spatial clustering application with noise (DBSCAN) was selected for object clustering considering its powerful performance on processing spatial points. The point p whether belongs to one cluster is determined by two parameters: searching radius (ε) and minimal points (MinPts). The ε is used to determine whether another point is the neighborhood (N) of p. The N containing the number of points (nN) equal to or larger than MinPts is considered as high density. Based on ε and MinPts, one point can be assigned to one of the three categories: core point ($p \in N$ & $nN \geq$ MinPts), border point ($p \epsilon N$ & $nN <$ MinPts), and noise point ($p \notin N$). A cluster contains core points and border points. The traditional DBSCAN using the fixed values of ε and MinPts could not cluster the points with varying density. For the points scanned by the roadside LiDAR, the density of points decreased with the increasing distance to LiDAR [37]. Therefore, it is difficult to cluster the points using fixed MinPts and ε. Dynamic parameters were then developed for DBSCAN considering the LiDAR sensor's mechanical structure and the features of LiDAR points. The primary criterion of the ε selection is to make sure points scanned by different beams (different heights) can be detected as the neighbor. Therefore,

$$\varepsilon \geq d \tag{1}$$

where d is the height difference between two adjacent laser beams. d can be estimated based on the distance between points to LiDAR [37]. A previous study [38] showed that the modified DBSCAN can achieve an accuracy of more than 97%.

The classification of one object is critical for the analysis of the vehicle-pedestrian conflict. It is necessary to know whether the object is a vehicle or a pedestrian. Since the LiDAR can generate the point cloud for its scanned object, the shape information can be generated for each object. The selected features used to distinguish the vehicles and pedestrians include the number of points, object length, height profile, the difference between height and length, and distance to the LiDAR. Those features can be automatically calculated from the LiDAR data. By comparing the performance of different classification methods including Naive Bayes, K-Nearest Neighbor, Support Vector Machine, Random Forest, and Backpropagation Artificial Neural Network, it was found that random forest can achieve the best performance with the relatively low computing cost [39]. The vehicles and pedestrians can then be successfully distinguished using random forest with the six features.

Lane information is another important part of HRMTD. Lane information plays a key role in the identification of vehicle-pedestrian conflicts. For example, the lane information can help identify whether the vehicle passed the road before the pedestrian crossing the road or after the pedestrian crossing the road. These two types of events should have different levels of risks (vehicles passing the road before the pedestrian crossing the road is more dangerous). This research used a density-based method for lane

identification [40]. It is assumed that the number of lane-changing vehicles is less than that of non-lane-changing vehicles. After aggregating multiple frames of vehicle points in the space, the vehicle points should be concentrated within each lane, which means the point density within the lane should be higher compared to that on the lane boundary. By applying the DBSCAN algorithm, the vehicle points located in the same lane can be grouped into one cluster. Then the boundary of each cluster can be considered as the boundary of the lane.

To generate the trajectory of one object, the target should be continuously tracked, which is also called object association. The object tracking should consider two factors: the distances between an object in a previous frame to all objects in the current frame and the time difference between two considered frames. Two objects were matched if the distance between them was the shortest among all the candidate objects within a certain time period. Then a discrete Kalman filter method was applied for object tracking. The position and the speed information of the object in the previous and the current frame were the input of the Kalman Filter to estimate the status of the object in the current frame. For some frames where clusters cannot be detected, the Kalman filter can be used to predict the status of the missing object, thus improving the tracking continuity [40].

B. TRAJECTORY EVALUATION

The trajectory of each road user can then be generated using the above-described procedure. Table 1 shows the summary of the elements of the trajectory from the roadside LiDAR. Figure 2 shows an example of trajectories extracted from the roadside LiDAR. The detailed trajectories made the analysis between the vehicles and pedestrians possible.

Before using the proposed data processing algorithm to extract the trajectories for the input of the vehicle-pedestrian conflict analysis, the performance of the data processing algorithm was firstly evaluated. Three elements (vehicle volume, pedestrian volume, and vehicle speed) were evaluated based on feasibility and simplicity. The vehicle volume and pedestrian volume were evaluated by the counting number of vehicles, the number of pedestrians in trajectories generated by the proposed algorithm, and comparing the results with the volume counted from a 360-degree camera. One-hour (10:30 am to 11:30 am) of traffic data was collected at a pedestrian crossing midblock of Baring Blvd in Sparks. This was used for evaluation. This site was selected since the pedestrian volume was high during the peak hours (11:00 am to 12:00 pm) based on the historical pedestrian volume counting results [41]. This site is located at the front of the Edward C Reed High School. The error rate can be calculated in Equation 2.

$$ER = \frac{|NL - NC|}{NC} \times 100\% \quad (2)$$

where ER is the error rate; NL is the number of traffic volume extracted from LiDAR data; NC is the number of traffic volume counted from the camera. Table 2 shows the results of volume evaluation.

The high pedestrian volume from 11:00 am to 11:30 am was caused by the students out for lunch after school. It was shown from 10:30 am to 11:00 am (non-peak time), the proposed method can achieve 100% accuracy and 96.9% for pedestrian volume counting and vehicle volume counting, respectively. The vehicle volume extracted from LiDAR data was higher than that counted from the camera, which was

TABLE 1. Elements in the trajectories.

Element Name	Description
Object ID*	The unique ID for the object
Object Type*	The class of the object. 1 represents "vehicle" and 2 represents "pedestrian".
Timestamp	The timestamp of the point closest to the LiDAR in the object-tracking point.
Object Length	The calculated length of the object
Object Width	The calculated width of the object
X	The x coordinate of the object (tracking point)
Y	The y coordinate of the object (tracking point)
Z	The z coordinate of the object (tracking point)
Direction	A value to represent the location of the target in a polar coordinate system.
Distance	The distance between the object and the roadside LiDAR
Longitude	The longitude of the object (optional)
Latitude	The latitude of the object (optional)
Elevation	The elevation of the object (optional)
Direction	The moving direction of the object
Lane	A value to represent the lane information (post-processed)
Speed	The speed of the object. Unit: mph for the vehicles and ft/s for the pedestrians
Frame Index	The frame ID of the object

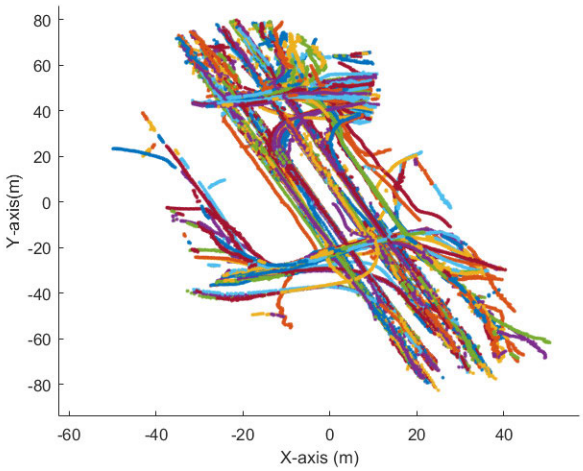

FIGURE 2. Example of trajectories extracted from roadside LiDAR.

TABLE 2. Traffic volumne evaluation.

Time period	Vehicle/Pedestrian	Counted from camera	Extracted from LiDAR data	Accuracy (%)
10:30 am to 11:00 am	Number of pedestrians	20	20	100
	Number of vehicles	230	223	96.9
11:00 am to 11:30 am	Number of pedestrians	402	389	96.8
	Number of vehicles	296	311	94.9

mainly caused by the occlusion issue. For example, one vehicle might be blocked by another vehicle and the blocked vehicle re-appeared after several frames. The blocked vehicle may discard its original ID and obtain a new one since the algorithm could not continuously track the same vehicle under this situation. The error got larger when the traffic got congested (error rate raised to 5.1% from 3.1%). The error in the pedestrian volume also got larger when the volume increased dramatically from 11:00 am. The algorithm may count two close-by pedestrians as one pedestrian if they walk side by side. Overall, the proposed data extraction method can achieve a relatively high accuracy to count pedestrian volume and vehicle volume.

The second site was selected at a parking lot to evaluate the speed of the vehicle calculated from the trajectory. The speed information was recorded using the On-Board Diagnostic System Information (OBD-II) logger from the vehicle. During the testing time, only the testing vehicle was in the parking lot, which can be easily matched to the corresponding vehicle in the LiDAR data. The speed recorded from the testing vehicle and from the LiDAR data were compared. Figure 3 shows two examples of the comparison results.

It was shown that the speed tracked using the LiDAR data can match the speed read from the logger well in general. To quantitively measure the speed difference from the speed from the logger and the LiDAR data, the cumulative difference in ten minutes was documented in Figure 4. It was shown that 98.8% of speed records from the logger and the LiDAR data had a difference of less than 2 mph.

The evaluation showed that the overall accuracy of the data processing algorithm was high, indicating the trajectories can be used for vehicle-pedestrian conflict analysis.

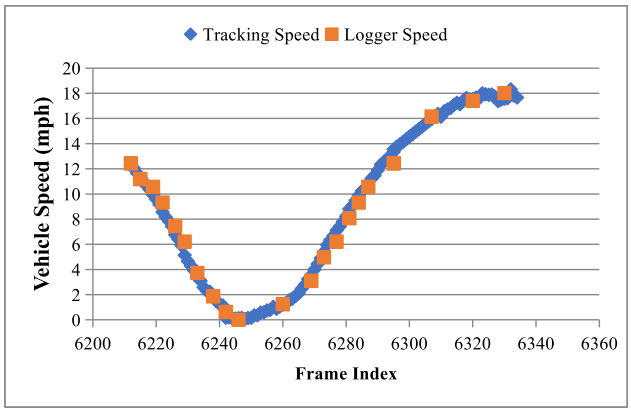

(a) Stop-and-Go Situation

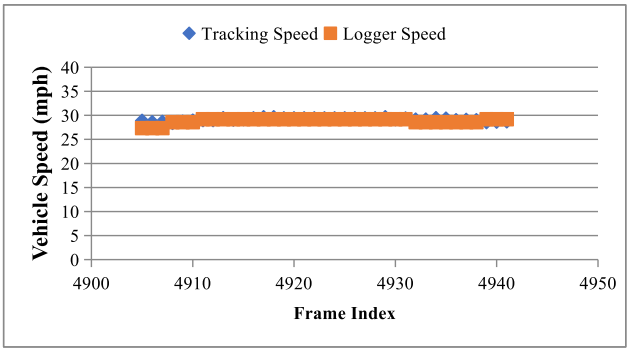

(b) Non-stop Situation

FIGURE 3. Speed evaluation.

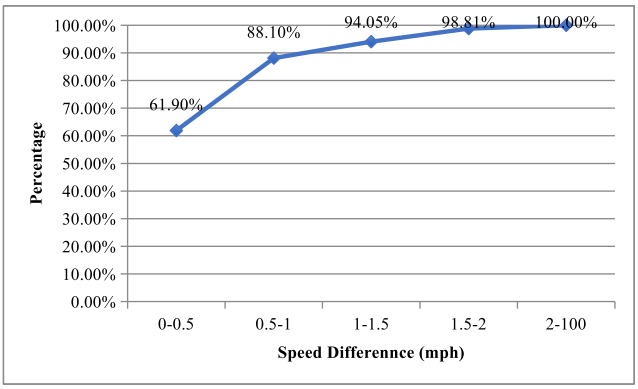

FIGURE 4. Speed difference distribution.

III. INDICATORS OF SURROGATE SAFETY MEASURESTES

A. THE DEVELOPED INDICATOR

There have been a lot of indicators developed for surrogate safety measure analysis. The indicators can be roughly divided into three groups: time-proximity indicators [42], evasive action-based indicators [43], and distance-based indicators [44]. Table 3 summarizes the major indicators of surrogate safety measures developed in previous studies.

It is shown in Table 3 that a lot of indicators (well known or less known) have been developed and used for safety surrogate measures. A previous study [46] compared the performance of different types of indicators and found that it is hard to say which indicator is better since the performance of different indicators varied at different investigating sites. For a sole indicator, it usually only suited a specific situation and one indicator usually had limited transferability. Therefore, the combined use of the indicators can be a good option to improve the accuracy of conflict analysis [47]. This paper developed a rule-based method using the speed-distance profile (SDP) of the vehicles for vehicle-pedestrian conflicts identification. The rule-based method can be

TABLE 3. Indicators of surrogate safety measures.

Time-proximity indicators				
	Equation or description	Required parameters	Threshold	Limitations
Time-to-collision (TTC)	The time that remains until a collision between two vehicles would have occurred if the collision course and speed difference are maintained.	Distance and speed	2.6 s [46]	Assumption about instant speed did not reflect the real situation [76].
Time Exposed Time-to-collision (TET)	The duration of exposition to safety-critical time-to-collision values over specified time duration	Time	19.5 s	If the TTC-value is lower than a threshold, TET value remains unchanged.
Time Integrated Time-to-collision (TIT)	The integral of the time-to-collision profile of drivers	Time		The accuracy of TIT calculation with the aid of the TTC-frequency distribution is low.
Post Encroachment Time (PET)	The extra time required in order to give the pedestrian a safety margin to allow for misjudgment or wrong estimate of the situation.	Time	2.5 s [13]	PET is only useful for measuring safety critical events where there are transversal trajectories for the road-users involved.
Deceleration Rate (DR) or Deceleration Rate to Avoid a Crash (DRAC)	The highest rate at which a vehicle must decelerate to avoid a collision.	Speed and distance	-1 m/s^2	The measurement of actual deceleration rates is difficult and resource demanding.
Evasive action-based indicators				
Absolute rate of the speed change in Step Frequency	The change of speed in the pedestrian's walking mechanism	Pedestrian speed	0.7 steps/s^2	The transferability was unknown
Jerks	Composite g-force and speed	Pedestrian speed and distance	-8 m/s^3	The transferability was unknown
Distance-based indicators				
Distance between stop position and pedestrian (DSPP) [13]	The distance between one vehicle and one pedestrian when the vehicle firstly stopped before reaching the pedestrian	Distance	1.2 m~6.1 m	DSPP did not consider the deceleration (speed change) in analysis
Proportion of Stopping Distance (PSD) [82]	The ratio of the distance available for a maneuver to that of the necessary braking distance to a projected point of collision	Distance	0.5	The transferability was unknown

considered as a combination of different types of indicators. The SDP in this paper is "the speed profile of a vehicle calculated with the distance between the vehicle and the pedestrian with a consistent time interval." The SDP can be described in Equation 3, as shown at the bottom of the this page, where t0 is the time when the pedestrian and the vehicle can both be detected firstly in the LiDAR; V represents the speed; XP, YP, ZP are the XYZ coordinate of the pedestrian; XV, YV, ZV are the XYZ coordinate of the vehicle; tI is the time when the trajectory of the pedestrian and the trajectory of the vehicle intersect; TI is the time interval. In Equation (3), as shown at the bottom of this page, TI equals to the time interval between the adjacent frames of the LiDAR data. The total number of records (N) can be calculated as

$$N = \frac{tI - t0}{F} + 1 \tag{4}$$

where F is the rotation frequency of the LiDAR. Figure 5 shows an example of SDP.

The green cycles in Figure 5 represent the SDP of a normal event (no conflicts) and the red squares represent the SDP of a near-crash (the vehicle did not yield to the pedestrian).

$$SDP = \begin{bmatrix} V_{t0} \sim \sqrt{(XP_{t0} - XV_{t0})^2 + (YP_{t0} - YV_{t0})^2 + (ZP_{t0} - ZV_{t0})^2} \\ V_{t0+TI} \sim \sqrt{(XP_{t0+TI} - XV_{t0+TI})^2 + (YP_{t0+TI} - YV_{t0+TI})^2 + (ZP_{t0+TI} - ZV_{t0+TI})^2} \\ \cdot \\ \cdot \\ \cdot \\ V_{tI} \sim \sqrt{(XP_{tI} - XV_{tI})^2 + (YP_{tI} - YV_{tI})^2 + (ZP_{tI} - ZV_{tI})^2} \end{bmatrix} \tag{3}$$

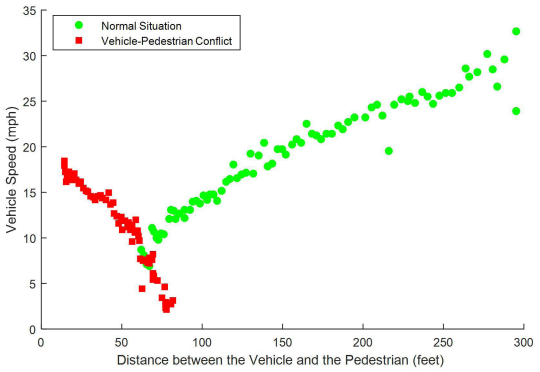

FIGURE 5. Examples of SDP.

Evidently, the SDPs of these two types of events are different. The technical difficulty here is how to assess the safety status based on the SDP. Each point (P) in Figure 5 represents the status of the vehicle at the specific timestamp. Given the speed of the vehicle at P is V_P and the deceleration of the vehicle (DC) is constant, the distance (D) required for deceleration before hitting the pedestrian can be calculated in Equation 5.

$$D = (\frac{V_p - V_i}{2}) \times T \tag{5}$$

where T is the time used for the vehicle moving from P to the intersection of vehicle and pedestrian trajectories. V_i is the vehicle speed at the intersection of vehicle and pedestrian trajectories. To avoid a crash, V_i should be equal to 0. Since DC was assumed to be constant, T can be easily calculated as

$$T = \frac{V_p - V_i}{DC} \tag{6}$$

Then Equation 5 can be revised as

$$D = \frac{V_p^2}{2 \times DC} \tag{7}$$

The max DCs recommended by the Institute of Transportation Engineers (ITE) Traffic Engineering Handbook and AASHTO are -3.0 m/s^2 and -3.4 m/s^2, respectively [48]. In this paper, we used the -3.4 m/s^2 as the acceptable DC. Assuming the distance of the vehicle and the pedestrian at P is DP, a vehicle-pedestrian crash can occur if

$$D \geq D_p \tag{8}$$

However, D did not consider the brake reaction distance (BRD). To give a more accurate calculation, the stopping sight distance (SSD) was used here. SSD is the minimum sight distance required along a roadway to enable a vehicle to stop before reaching a stationary object in its path. SSD can be represented as

$$SSD = 0.278V \times t + 0.039V^2/DC \tag{9}$$

where V is the vehicle speed, t is brake reaction time, and DC is the deceleration rate. The traditional SSD used the design speed for calculation. In the real situation, the actual speed can be offset from the design speed under different traffic situations. With the trajectory data extracted from the LiDAR, the actual speed of the vehicles can be obtained. Therefore, the SSD used in this paper can be considered as an improved version of the traditional one. The design standards of the American Association of State Highway and Transportation Officials (AASHTO) use 1.5 seconds for perception time and 1.0 second for reaction time [49]. Therefore, t is assumed as 2.5 seconds in this research. DC was selected as 3.4m/s^2.

TABLE 4. Near-Crash identification using SDP.

Normal Behavior	$SSD - LTC \leq D_p$
Crash Relevant	$SSD - LTC > D_p$ & $SSD \leq D_p$
Near Crash	$SSD > D_p$

Therefore, SSD can be simplified:

$$SSD = 0.695V + 0.011V^2 \tag{10}$$

The engineers or researchers can choose their own values for DC and t based on different purposes. In other words, the SSD can be customized based on the requirements of different users. Even if SSD is less than DP, pedestrians may still feel in danger or uncomfortable if the distance between the vehicle and the pedestrian is short. As introduced in the previous paper [13], the vehicle should stop before the yield/stop line to avoid any uncomfortable feeling to the pedestrians. The distance between yield/stop line to crosswalk (LTC) varied based on different control types of the intersections (e.g. signalized midblock crosswalk-40ft; uncontrolled midblock crosswalk-9.1 meters) [50]. If the vehicle could not stop before the crosswalk, then the event can be considered as near crash. The near crash refers to the event that should be avoided since, by definition, a successful, last-second evasive maneuver is needed to avoid a crash. If the vehicle stopped between the crosswalk and the yield/stop line, this event can be considered as crash relevant. The crash relevant in this paper can be defined as the event that requires a crash avoidance response that is less severe than a rapid evasive maneuver, but greater in severity than a normal maneuver. The crash relevant may also cause the pedestrian to feel uncomfortable. Therefore, vehicle-pedestrian conflicts can be identified using the criteria in Table 4.

The SDP considered the brake time, vehicle speed, distance, and deceleration for near-crash identification. The only missing part was the evasive action of the pedestrian. This was due to the variance in the speed calculation. The previous study found that it's difficult to track the pedestrian's speed accurately using the roadside LiDAR due to the occlusion issue [13].

If the pedestrian did not reach the boundary of the intersection, the vehicle using the lane close to the pedestrian may not slow down. This case should be considered as a normal event.

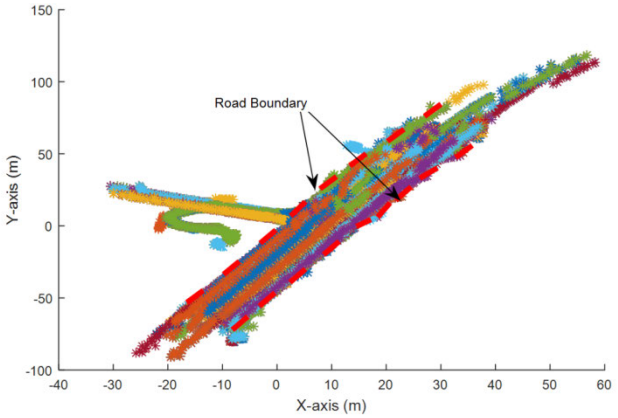

FIGURE 6. ROI selection.

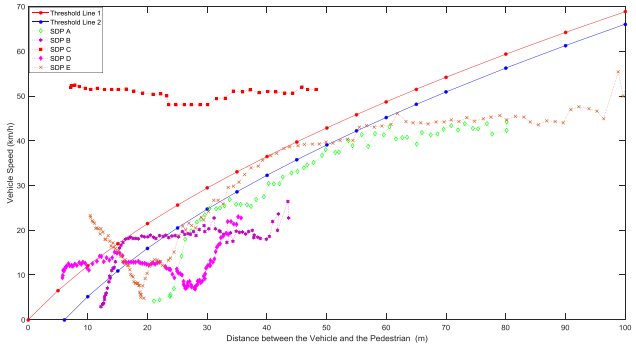

FIGURE 7. Example of SDPs.

However, using the rule-based method can identify this case as a near crash or crash relevant. To reduce the false reports, we set a region of interest (ROI) for the analyzing area. The road boundary was used as the ROI here. Figure 6 shows an example of ROI (only on the major road). We only focused on the pedestrians and vehicles within the road boundaries.

Figure 7 shows several SDPs collected at Baring Blvd in Reno.

The threshold line 1 was generated based on Table 4 to distinguish near crash and crash relevant, and the threshold line 2 was used to distinguish crash relevant and normal behavior. The whole space can then be divided into three parts. Below the threshold line 2, this area means that drivers can stop before reaching the LTC with the max deceleration rate-3.4m/s^2 and the reaction time -2.5s. Between threshold line 1 and 2, this area means that drivers can stop but could take a longer distance. Any event located in this area can be considered as crash relevant. Above the threshold line 1, this area means that the drivers are more likely to hit the pedestrian and the drivers may need to brake sharply to avoid the potential crash, which means near-crash occurs. In Figure 7, there were five different SDPs (A, B, C, D, E), SDP A was located in the area below the threshold line 2, which means this was a normal event (no risks for the pedestrian). SDP B was originally located in the area below the threshold line 2 (the speed was relatively low), but the drivers did not

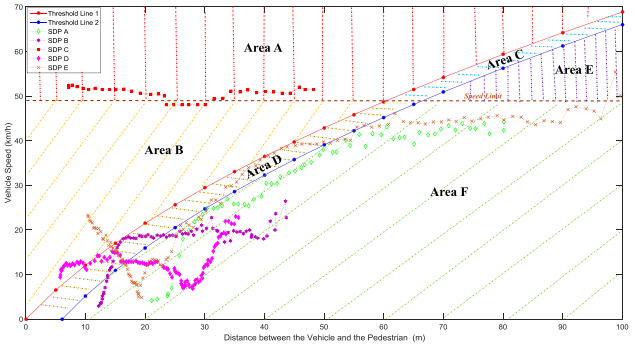

FIGURE 8. Different risk levels in SDP.

slow down until about 16 meters away from the pedestrian. As a result, the SDP reached the area between threshold line 1 and 2. This situation was considered as a crash-relevant event. SDP C was totally above the threshold line 2 and the vehicle did not slow down to yield to the pedestrian. Though this event did not lead to a crash eventually, the aggressive driving behavior could be potentially dangerous for the pedestrians. SDP D represented a situation where the vehicle slowed down a little at a distance of about 27m from the pedestrian, then the vehicle moved forward with relatively low speed but did not fully stop though the distance between the pedestrian and the vehicle was short. SDP E represented a situation where a vehicle slowed down (almost stopped) at a distance of about 19m from the pedestrian. Then the driver decided to speed up. This was another type of dangerous driving behavior. However, in Figure 7, one missing factor was the speed limit. Any behavior above the speed limit or above a specific value (e.g. 5%∼10% above the speed limit) can be dangerous though they may be located in the area below the threshold line 2. To address this issue, the speed limit was involved in the SDP chart. Then Figure 7 can be plotted as Figure 8. Figure 8 was divided into six subareas (Area A, B, C, D, E, F) using the speed limit line and the threshold lines 1 and 2. In Figure 8, area A has the highest level of crash risk. The speed of the vehicle located in Area A was higher than the speed limit, and the distance between the vehicle and the pedestrian was shorter than SSD. For area B, the speed of the vehicle was lower than the speed limit but the distance between the vehicle and the pedestrian was still shorter than SSD. The risk of the event with SDP located in area B was lower than that in area A. The same rule can be applied to areas C, D, E, and F. Area F has the lowest level of crash risk. The speed of the vehicle located in area F was lower than the speed limit and the distance between the vehicle and the pedestrian was longer than SSD plus LTC. For an SDP, it may cross different areas in Figure 7 or Figure 8. The final level was selected based on the most dangerous area where the SDP was located. For most situations, the traffic engineers may not need to have such detailed levels for the crash risk. Therefore, the rules shown in Figure 7 can usually meet the requirements of most users.

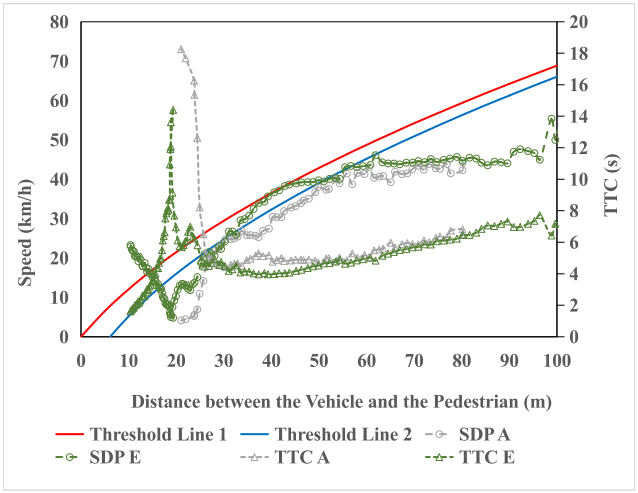

FIGURE 9. SDP and TTC.

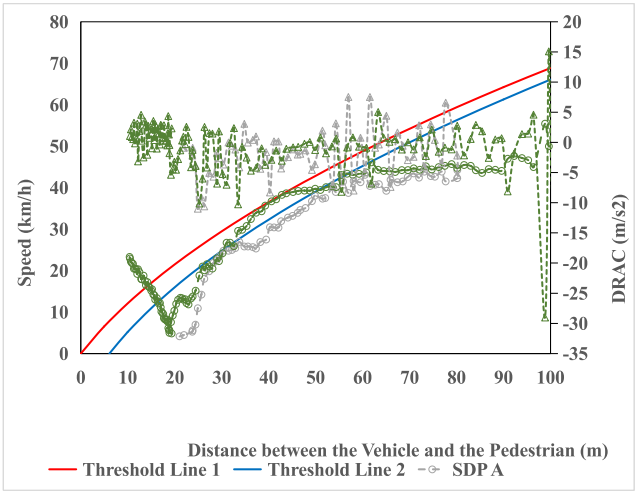

FIGURE 10. SDP and DRAC.

B. EXTENDED USE OF TRAJECTORIES

For some researchers or traffic engineers, they may prefer the widely used indicators (e.g. TTC or DRAC). In fact, those indicators can all be generated from the trajectories. The following parts of this subsection show the calculation of those indicators from the SDP.

The TTC can be calculated as

$$\mathrm{TTC} = \frac{\mathrm{D}}{\mathrm{V}} \tag{11}$$

where D is the distance between the vehicle and the pedestrian and V is the vehicle speed. Figure 9 shows the TTC calculation results of SDP A and E.

It can be seen that for each SDP, the corresponding TTCs can be easily calculated.

The DRAC can be easily calculated in Equation 12.

$$\mathrm{DRAC} = (\mathrm{V_t} - \mathrm{V_{t+1}})/\mathrm{T} \tag{12}$$

where Vt represents the vehicle speed at frame t. T is the time interval between two adjacent frames. Figure 10 shows the DRAC calculation results of SDP A and E.

It can be seen that for each SDP, the corresponding DRACs can be easily calculated. The other indicators can also be calculated from the SDP or from the trajectories. This means that our proposed procedure can be used to generate different indicators based on the requirement of different users. Another thing should be noted here is that the law of some states (such as Nevada) requires the vehicles waiting at the intersection until the pedestrians finished crossing the intersection. This means that if the vehicle starts to move before the pedestrian finish as his/her crossing, then the drivers will break the law. The level of this kind of risk may not be as high as near-crash. But the traffic engineers or researchers may want to know the number of these kinds of events. These types of events can be identified using the following procedure. Assuming the pedestrian reached the road boundary at Ta and finished crossing the road at Tb, and the vehicle passed the crosswalk

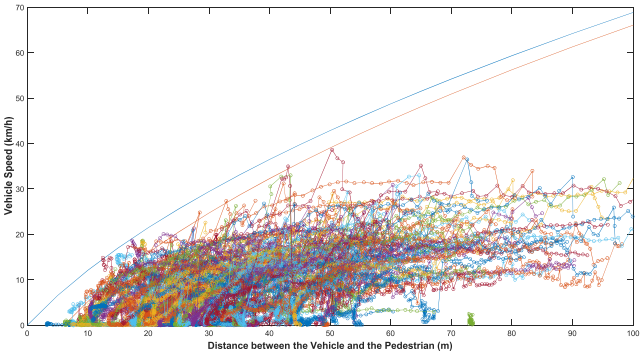

FIGURE 11. SDPs of normal events.

at Tc, these kinds of events meet the following criteria:

$$\mathrm{Ta} < \mathrm{Tc} < \mathrm{Tb} \tag{13}$$

The time information was not covered in the SDP but was stored in the trajectory data, as shown in Appendix A. Therefore, extracting ''breaking the law'' events from the trajectories is possible.

IV. CASE STUDY

To evaluate the performance of the proposed method, the proposed method was applied to the data collected at an unsignalized crosswalk at Baring Blvd in Reno. The LTC was selected as 6.1m and the break time was set as 2.5 s. The rotating frequency of the LiDAR was set as 10 Hz. A total of 235 normal events were manually extracted from the Veloview- a visualization software to show the raw LiDAR data in a local system. The normal events were selected based on the adjustment of the data analyst at the University of Nevada, Reno (UNR). Figure 11 shows the results of the SDPs of those normal events.

In Figure 11, a total of 15 events was located between the two threshold lines, meaning they were identified as crash relevant. It should be mentioned that the bias between the results of the SDPs and the LiDAR video was inevitable.

TABLE 5. Near-Crash identification with two different methods.

	Ground True Data	Proposed Method	Method in [13]
Number of Near-Crash Events	57	57	51
Accuracy		100%	89.5%

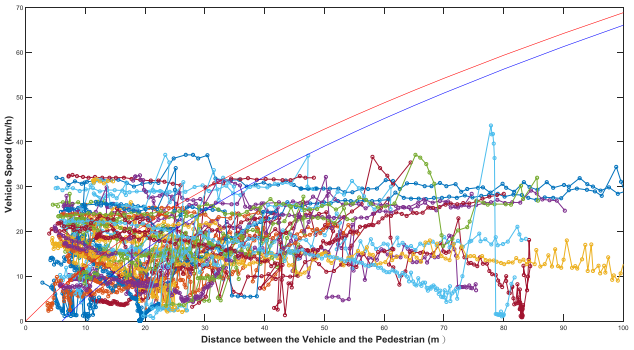

FIGURE 12. SDPs of near crash events.

The difference rate was 6.4%, which was acceptable. It can be also seen that the variance of the calculated speed was high when the vehicle was far away from the LiDAR and went smaller when the vehicle moved close to the LiDAR. Those variances can also influence the accuracy of the rule-based method.

A total of 57 near crashes were manually identified by the data analyst. The selection criteria were fuzzy and were selected based on the information provided by the Strategic Highway Research Program (SHRP 2) Naturalistic Driving Study InSight Data Access Website-https://insight.shrp2nds.us. Those events were then checked using the rule-based method. Figure 12 shows the SDPs of those events.

It is shown that all the 57 events had part of the SDP located above the red threshold line. In other words, all the 57 events were identified as near-crashes by the proposed method. The case study shows that the proposed method can be used to identify the vehicle-pedestrian near-crash events though there were some misidentifications between normal events and crash relevant events.

To further evaluate the performance of the proposed method, this paper used the method developed in [13] to process the data collected at the same unsignalized crosswalk at Baring Blvd in Reno. The thresholds for near-crash were illustrated as follows: TDPI $<$ 2.5 or 0 $<$ DSPP $<$ 6.1m or vehicle speed within area A in speed-distance profile (See Figure 5 in [13]). Table 5 shows the results of the two methods.

It was shown that the proposed method can successfully extract all the 57 near-crash events while the method in [13] can only extract 51 near-crash events (89.5%). The proposed method considered the distance between the vehicle and the pedestrian, vehicle speed, deceleration, and driver reaction time in the algorithm, and therefore provided accuracy for near-crash identification compared to the method in [13].

V. DISCUSSION

The focus of this paper was through the vehicle aspect, which means all the indicators were developed based on the features of vehicles and drivers. The pedestrian side was not well addressed. This is mainly caused by the variance in the pedestrian speed. A 1.0 km/h variance in vehicle speed may not be a big problem, but the same variance in pedestrian speed can cause a big problem for evasive action identification. Therefore, at this stage, we did not analyze the behavior of the pedestrian. The future studies should improve the accuracy of the trajectories extracted from the roadside LiDAR. The previous study also found that pedestrians prefer to finish crossing as soon as possible when he/she perceives potential risk [51]. Therefore, it will be an interesting topic to validate the behavior change of the pedestrian under potential risks.

All the recommended values in this paper were based on the features of light-duty small vehicles. The deceleration features of the trucks should be dramatically different. Further studies should focus on how to provide the thresholds for indicators regarding truck-pedestrian crashes. This paper shows the ability of LiDAR using high-resolution trajectories for vehicle-pedestrian near-crash identification. A similar idea can be extended to vehicle-vehicle conflict analysis. Since the trajectories can be generated in real-time, the rule-based vehicle-pedestrian conflict identification method can be implemented for the crash-avoidance system development. The previous study found that earlier warning leads to shorter reaction times and lower deceleration rates [52]. Therefore, our research can help improve pedestrian safety by detecting the near-crash events and broadcasting warning information through Infrastructure to Vehicle (I2V) communication.

VI. CONCLUSION

This paper developed a systematic method for vehicle-pedestrian conflicts identification using the HRMTD extracted from the roadside LiDAR data. The HRMTD can be successfully generated using the LiDAR data processing procedure. The developed SDP-an indicator for surrogate safety measure can illustrate the status of the vehicle-pedestrian conflict vividly. The case study in Reno showed the effectiveness of using the SDP for vehicle-pedestrian conflicts identification. The other indicators such as TTC or PET can also be calculated from the trajectory data. The proposed method can extract near-crash events with higher accuracy compared to the state-of-the-art method. Besides traffic safety, driver behavior analysis, fuel consumption analysis and other transportation aspects can all benefit from the HRMTD.

As mentioned before, all the recommended values in this paper can be adjusted by the engineers based on their own requirements. This paper used the raw LiDAR data (shown in visualization software) to evaluate the performance of

the proposed method. Further studies should consider using video data to further evaluate the proposed method.

ACKNOWLEDGMENT

(Renjuan Sun and Rui Yue contributed equally to this work.)

REFERENCES

[1] Y. Malinovskiy, Y. J. Wu, and Y. Wang, "Video-based monitoring of pedestrian movements at signalized intersections," *Transp. Res. Rec.*, vol. 2073, no. 1, pp. 11–17, 2008.

[2] National Center for Statistics and Analysis, "Police-reported motor vehicle traffic crashes in 2017 (Traffic Safety Facts Research Note," Nat. Highway Traffic Saf. Admin., Washington, DC, USA, Tech. Rep. HS 812 696, Apr. 2019.

[3] F. Guo, "Near crashes as crash surrogate for naturalistic driving studies," *Transp. Res. Rec., J. Transp. Res. Board*, vol. 2147, no. 1, pp. 66–74, 2010.

[4] D. S. Pawar, V. Kumar, N. Singh, and G. R. Patil, "Analysis of dilemma zone for pedestrians at high-speed uncontrolled midblock crossing," *Transp. Res. C, Emerg. Technol.*, vol. 70, pp. 42–52, Sep. 2016.

[5] K. Fitzpatrick, S. Turner, and M. A. Brewer, "Improving pedestrian safety at unsignalized intersections," *ITE J.*, vol. 77, no. 5, pp. 34–41, 2007.

[6] J. Wu and H. Xu, "Driver behavior analysis for right-turn drivers at signalized intersections using SHRP 2 naturalistic driving study data," *J. Saf. Res.*, vol. 63, pp. 177–185, Dec. 2017.

[7] C. Lee and M. Abdel-Aty, "Comprehensive analysis of vehicle–pedestrian crashes at intersections in Florida," *Accident Anal. Prevention*, vol. 37, no. 4, pp. 775–786, 2005.

[8] J. Wang, Y. Zheng, X. Li, C. Yu, K. Kodaka, and K. Li, "Driving risk assessment using near-crash database through data mining of tree-based model," *Accident Anal. Prevention*, vol. 84, pp. 54–64, Nov. 2015.

[9] D. Lord, "Analysis of pedestrian conflicts with left-turning traffic," *Transp. Res. Rec.*, vol. 1538, no. 1, pp. 61–67, 1996.

[10] A. Talebpour, H. S. Mahmassani, F. Mete, and S. H. Hamdar, "Near-crash identification in a connected vehicle environment," *Transp. Res. Rec.*, vol. 2424, no. 1, pp. 20–28, 2014.

[11] A. Sobhani, W. Young, and M. Sarvi, "A simulation based approach to assess the safety performance of road locations," *Transp. Res. C, Emerging Technol.*, vol. 32, pp. 144–158, Jul. 2013.

[12] N. Arbabzadeh, M. Jafari, M. Jalayer, S. Jiang, and M. Kharbeche, "A hybrid approach for identifying factors affecting driver reaction time using naturalistic driving data," *Transp. Res. C, Emerging Technol.*, vol. 100, pp. 107–124, Mar. 2019.

[13] J. Wu, H. Xu, Y. Zheng, and Z. Tian, "A novel method of vehicle-pedestrian near-crash identification with roadside LiDAR data," *Accident Anal. Prevention*, vol. 121, pp. 238–249, Dec. 2018.

[14] A. Laureshyn, Å. Svensson, and C. Hydén, "Evaluation of traffic safety, based on micro-level behavioural data: Theoretical framework and first implementation," *Accident Anal. Prevention*, vol. 42, no. 6, pp. 1637–1646, 2010.

[15] T. Sayed, M. H. Zaki, and J. Autey, "Automated safety diagnosis of vehicle–bicycle interactions using computer vision analysis," *Saf. Sci.*, vol. 59, pp. 163–172, Nov. 2013.

[16] K. Ismail, T. Sayed, N. Saunier, and C. Lim, "Automated analysis of pedestrian-vehicle conflicts using video data," *Transp. Res. Rec. J. Transp. Res. Board*, vol. 2140, no. 1, pp. 44–54, Dec. 2009.

[17] X. Jiang, W. Wang, and K. Bengler, "Intercultural analyses of time-to-collision in vehicle–pedestrian conflict on an urban midblock crosswalk," *IEEE Trans. Intell. Transp. Syst.*, vol. 16, no. 2, pp. 1048–1053, Apr. 2015.

[18] A. Tageldin and T. Sayed, "Developing evasive action-based indicators for identifying pedestrian conflicts in less organized traffic environments," *J. Adv. Transp.*, vol. 50, no. 6, pp. 1193–1208, 2016.

[19] F. Huguenin, A. Torday, and A. Dumont, "Evaluation of traffic safety using microsimulation," in *Proc. 5th Swiss Transp. Res. Conf. (STRC)*, Ascona, Swiss, Mar. 2005, pp. 1–18.

[20] D. Gettman and L. Head, "Surrogate safety measures from traffic simulation models," *Transp. Res. Rec.*, vol. 1840, no. 1, pp. 104–115, 2003.

[21] K. Ozbay, H. Yang, B. Bartin, and S. Mudigonda, "Derivation and validation of new simulation-based surrogate safety measure," *Transp. Res. Rec.*, vol. 2083, no. 1, pp. 105–113, 2008.

[22] C. Wang and N. Stamatiadis, "Surrogate safety measure for simulation-based conflict study," *Transp. Res. Rec.*, vol. 2386, no. 1, pp. 72–80, 2013.

[23] Y. Guo, M. Essa, T. Sayed, M. M. Haque, and S. Washington, "A comparison between simulated and field-measured conflicts for safety assessment of signalized intersections in Australia," *Transp. Res. C, Emerg. Technol.*, vol. 101, pp. 96–110, Apr. 2019.

[24] J. Wu and H. Xu, "Driver behavior analysis on rural 2-lane, 2-way highways using SHRP 2 NDS data," *Traffic Injury Prevention*, vol. 19, no. 8, pp. 838–843, 2018.

[25] K.-F. Wu and P. P. Jovanis, "Defining and screening crash surrogate events using naturalistic driving data," *Accident Anal. Prevention*, vol. 61, pp. 10–22, Dec. 2013.

[26] Y. Sun, H. Xu, J. Wu, J. Zheng, and K. M. Dietrich, "3-D data processing to extract vehicle trajectories from roadside LiDAR data," *Transp. Res. Rec.*, vol. 2672, no. 45, pp. 14–22, Dec. 2018.

[27] J. Wu, "An automatic procedure for vehicle tracking with a roadside LiDAR sensor," *ITE J.-Inst. Transp. Eng.*, vol. 88, no. 11 pp. 32–37, Nov. 2018.

[28] J. Wu, H. Xu, J. Zheng, and J. Zhao, "Automatic vehicle detection with roadside LiDAR data under rainy and snowy conditions," *IEEE Intell. Transp. Syst. Mag.*, to be published.

[29] A. P. Tarko, K. B. Ariyur, M. Romero, V. K. Bandaru, and C. L. Jimenez, "Guaranteed LiDAR-aided multi-object tracking at road intersections: USDOT region V regional university transportation center final report," Purdue Univ., West Lafayette, IN, USA, Tech. Rep. 145PUY2, 2016.

[30] J. Zhao, H. Xu, H. Liu, J. Wu, Y. Zheng, and D. Wu, "Detection and tracking of pedestrians and vehicles using roadside LiDAR sensors," *Transp. Res. C, Emerg. Technol.*, vol. 100, pp. 68–87, Mar. 2019.

[31] Z. Y. Zhang, J. Zheng, X. Wang, and X. Fan, "Background filtering and vehicle detection with roadside lidar based on point association," in *Proc. 37th Chin. Control Conf. (CCC)*, Jul. 2018, pp. 7938–7943.

[32] B. Coifman, M. Wu, K. Redmill, and D. A. Thornton, "Collecting ambient vehicle trajectories from an instrumented probe vehicle: High quality data for microscopic traffic flow studies," *Transp. Res. C, Emerg. Technol.*, vol. 72, pp. 254–271, Nov. 2016.

[33] J. Wu, Y. Tian, H. Xu, R. Yue, A. Wang, and X. Song, "Automatic ground points filtering of roadside LiDAR data using a channel-based filtering algorithm," *Opt. Laser Technol.*, vol. 115, pp. 374–383, Jul. 2019.

[34] J. Wu, H. Xu, and W. Liu, "Points registration for roadside LiDAR sensors," *Transp. Res. Rec.*, vol. 2673, no. 9, pp. 627–639, 2019.

[35] J. Wu, H. Xu, and J. Zheng, "Automatic background filtering and lane identification with roadside LiDAR data," in *Proc. IEEE 20th Int. Conf. Intell. Transp. Syst. (ITSC)*, Oct. 2017, pp. 1–6.

[36] B. Lv, H. Xu, J. Wu, Y. Tian, and C. Yuan, "Raster-based background filtering for roadside LiDAR data," *IEEE Access*, vol. 7, pp. 76779–76788, 2019.

[37] J. Chen, H. Xu, J. Wu, R. Yue, C. Yuan, and L. Wang, "Deer crossing road detection with roadside LiDAR sensor," *IEEE Aceess*, vol. 7, pp. 65944–65954, 2019.

[38] Z. Zhang, J. Zheng, H. Xu, and X. Wang, "Vehicle detection and tracking in complex traffic circumstances with roadside LiDAR," *Transp. Res. Rec.*, vol. 2673, no. 9, pp. 62–71, 2019.

[39] J. Wu, H. Xu, Y. Zheng, Y. Zhang, B. Lv, and Z. Tian, "Automatic vehicle classification using roadside LiDAR data," *Transp. Res. Rec.*, vol. 2673, vol. 6, pp. 153–164, 2019.

[40] Y. Cui, H. Xu, J. Wu, Y. Sun, and J. Zhao, "Automatic vehicle tracking with roadside LiDAR data for the connected-vehicles system," *IEEE Intell. Syst.*, vol. 34, no. 3, pp. 44–51, May/Jun. 2019.

[41] *Nevada Department of Transportation*. Accessed: May 11, 2019. [Online]. Available: https://www.nevadadot.com/doing-business/about-ndot/ndot-divisions/planning/traffic-information

[42] Z. Fang, Q. Li, Q. Li, L. D. Han, and S.-L. Shaw, "A space–time efficiency model for optimizing intra-intersection vehicle–pedestrian evacuation movements," *Transp. Res. C, Emerg. Technol.*, vol. 31, pp. 112–130, Jun. 2013.

[43] Y. Guo, T. Sayed, and M. H. Zaki, "Exploring evasive action–based indicators for PTW conflicts in shared traffic facility environments," *J. Transp. Eng., A, Syst.*, vol. 144, no. 11, 2018, Art. no. 04018065.

[44] J. Wu and H. Xu, "Annual average daily traffic prediction model for minor roads at intersections," *J. Transp. Eng., A, Syst.*, vol. 145, no. 10, 2019, Art. no. 04019041.

[45] J. H. Hogema and W. H. Janssen, "Effect of intelligent cruise control on driving behaviour," TNO Hum. Factors, Soesterberg, The Netherlands, Tech. Rep. TM-1996-C-12, 1996.

[46] A. Tageldin, T. Sayed, and K. Shaaban, "Comparison of time-proximity and evasive action conflict measures: Case studies from five cities," *Transp. Res. Rec.*, vol. 2661, no. 1, pp. 19–29, 2017.
[47] A. P. Tarko, "Use of crash surrogates and exceedance statistics to estimate road safety," *Accident Anal. Prevention*, vol. 45, pp. 230–240, Mar. 2012.
[48] H. Xu and J. Wu, "Use of Naturalistic Driving Study data to determine right-turn driver deceleration behavior at signalized intersections, in *Proc. 97th Transp. Res. Board Annu. Meeting*, 2018, Art. no. 01877.
[49] G. T. Taoka, "Brake reaction times of unalerted drivers," *ITE J.*, vol. 59, no. 3, pp. 19–21, 1989.
[50] *Manual on Uniform Traffic Control Devices*, Federal Highway Administration, Washington, DC, USA, 2009.
[51] W. Zeng, P. Chen, H. Nakamura, and M. Iryo-Asano, "Application of social force model to pedestrian behavior analysis at signalized crosswalk," *Transp. Res. C, Emerg. Technol.*, vol. 40, pp. 143–159, Mar. 2014.
[52] X. Yan, Y. Zhang, and L. Ma, "The influence of in-vehicle speech warning timing on drivers' collision avoidance performance at signalized intersections," *Transp. Res. C, Emerg. Technol.*, vol. 51, pp. 231–242, Feb. 2015.

BIN LV received the B.S. degree in automatic control from the Lanzhou Railway Institute, Lanzhou, China, in 1998, and the M.S. and Ph.D. degrees in transportation planning and management with Lanzhou Jiaotong University, Lanzhou, in 2003 and 2012, respectively. He is currently a Professor with Lanzhou Jiaotong University. His research interests include traffic signal control, intelligent transportation systems, and traffic big data.

RENJUAN SUN received the B.S. and M.S. degrees from Shandong University, China, in 1995 and 2004, respectively, and the Ph.D. degree from Inha University, South Korea. She is currently a Professor with the School of Qilu Transportation, Shandong University. Her research interests include traffic safety, smart materials, and new concrete materials development.

HONGBO ZHANG received the B.S. and M.S. degrees in civil engineering from Shandong University, Jinan, China, in 2000 and 2003, respectively, and the Ph.D. degree from the Department of Civil Engineering, Tongji University, Shanghai, China, in 2006. He is currently an Associated Professor with Shandong University. His research interests include geotechnique engineering, road engineering, and traffic safety.

HAO XU received the bachelor's and master's degrees from the Department of Automation, University of Science and Technology of China, in 2004 and 2007, respectively, and the master's and Ph.D. degrees in civil engineering from Texas Tech University, in 2009 and 2010, respectively. From 2010 to 2013, he was a Postdoctoral Research Associate with Texas Tech University. Since 2013, he has been an Assistant Professor with the Department of Civil and Environmental Engineering, University of Nevada, Reno. His research interests include connected-vehicle applications with roadside LiDAR sensors, driving behavior analysis, traffic safety, and fuel consumption evaluation. He manages the connected-vehicle testing environment at the University of Nevada, Reno. The testing environment promotes interdisciplinary research on connected/autonomous vehicles to improve traffic safety and mobility. His research team has set up a LiDAR-based connected intersection in Reno, Nevada, and is performing research on LiDAR-based connected infrastructures.

RUI YUE received the B.S. degree from Beijing Jiaotong University, in 2015, and the M.S. degree from the University of Nevada, Reno, in 2017, where he is currently pursuing the Ph.D. degree with the Department of Civil and Environment Engineering. His research interests include traffic signal control, traffic operations, and GIS application in transportation.